

ARTICLE OPEN



Enhancing power factor of SnSe sheet with grain boundary by doping germanium or silicon

Jie Sun¹, Jiabing Yu², Yaguang Guo¹ and Qian Wang¹✉

Grain boundaries (GBs) widely exist in two-dimensional (2D) and three-dimensional (3D) materials in experiment, which significantly affect the thermoelectric performance because of the scattering effect on the transport of both electron and phonon. Motivated by the research progress in 3D SnSe, we have systematically studied the GBs in a SnSe monolayer including their stable geometric configurations, the effect of GBs on power factor and Seebeck coefficient, and the strategies to improve the performance by using first principles calculations combined with semiclassical Boltzmann theory. We find that the GBs increase the potential energy barrier of carriers and decrease the valley degeneracy of the conducting bands, leading to the reduction of Seebeck coefficient, as compared to that of the pristine SnSe sheet. We further demonstrate that the trapping gap states are effectively eliminated or reduced by doping germanium or silicon, leading to the enhanced electrical conductivity, power factor, and Seebeck coefficient. These findings shed lights on developing practical strategies for modulating the thermoelectric performance of 2D polycrystalline sheets.

npj Computational Materials (2020)6:99; <https://doi.org/10.1038/s41524-020-00368-6>

INTRODUCTION

Thermoelectric materials have attracted worldwide attention in the last few decades because they can directly harvest electricity from waste heat. Among them, tin selenide (SnSe) single crystal is most well-known for its astonishing high ZT values of 2.6 ± 0.3 at 923 K and 2.8 ± 0.5 at 773 K^{1,2}. However, the high cost of synthesizing SnSe *single crystal* and its poor mechanical properties impede the practical applications of this material. Therefore, many studies have been carried out for studying the thermoelectric performance of 3D *polycrystalline* SnSe^{3–9} and 2D SnSe¹⁰. It has been found that the ZT value of polycrystalline SnSe is dramatically reduced as compared to that of single-crystal SnSe because of the existence of grain boundaries (GBs) in polycrystalline structures, which can reduce the electrical conductivity. For example, GBs decrease the number of carriers in 3D p-type polycrystalline SnSe, leading to the poor electrical conductivity and poor thermoelectric performance¹¹. Also, in n-type 3D polycrystalline SnSe, the carrier concentration is reduced as compared with that of single crystalline SnSe⁷. To improve the performance, chemical doping has been used. Previous studies have shown that alkali elements^{3–5}, halogens^{6,7}, and Ag^{8,9} are the promising dopants for increasing the ZT value of 3D polycrystalline SnSe. For instance, the ZT value of K-doped polycrystalline SnSe is 1.1 at 773 K⁵, which is more than twice the original value of pure polycrystalline SnSe (0.5) at 823 K¹², but still much less than that (2.6–2.8) of its single crystal counterpart.

For SnSe thin films and nanosheets, the ZT values have been experimentally found to be relatively low, the maximum value can only reach 0.28 at 675 K^{13,14}, and the underlying reasons remain unclear. As a matter of fact, GBs have been found to exist in many 2D materials^{15–18}. However, the study on the effect of GBs on the thermoelectric properties of 2D SnSe has not been reported, although significant research progress has been made in 3D SnSe with GBs. To explore the mechanism of low ZT value of 2D SnSe, it is essential to address the following fundamental questions: (1)

what are the stable GB configurations in 2D SnSe? (2) How does GB affect the thermoelectric performance of 2D SnSe? (3) What are the strategies for improving the thermoelectric performance? To this end, we carry out a systematic theoretical study. Our results show that the GBs in 2D SnSe result in the defect trapping gap states inside the band gap, which impede the mobility of carriers. Doping with Ge or Si atoms can eliminate or reduce the trapping gap states, leading to a narrow band gap, an enhanced band convergence, and an improved electrical conductivity. These features, together with the reduced thermal conductivity, endow the 2D SnSe sheet containing GBs with improved thermoelectric performance.

RESULTS AND DISCUSSION

Geometric structures

Unlike other 2D materials with well-characterized GB structures such as in graphene¹⁵, boron nitride¹⁶, phosphorene¹⁷, and MoS₂¹⁸, the GB configurations in SnSe monolayer are still unclear. We first need to determine the stable GB configurations in the 2D SnSe. To this end, we use the coincident-site-lattice (CSL) theory¹⁹ that has been widely applied to determine the GB configurations in many materials^{20–22}, and find three stable GB configurations with the grain orientation angles of 37.76°, 54.32°, and 91.48°, as shown in Fig. 1, where the [010] and [001] directions are chosen to be the GB edge and rotation axis, respectively. The density of GB is determined by the distance between two neighboring GBs, the larger distance leads to the lower GB density. Taking monolayer SnSe with 91.48° GB as an example, we choose structures with different distances between two neighboring GBs to calculate their GB energies. The result is shown in Supplementary Fig. 1. When the distance between the two neighboring GBs reaches 21.49 Å, the GB energy converges to 0.21 eV, which means when the set distances are larger than 21.49 Å, the GB density will not be a main factor affecting the properties. To avoid the coupling

¹Center for Applied Physics and Technology, Department of Materials Science and Engineering, HEDPS, College of Engineering, Peking University, Beijing 100871, China. ²College of Optoelectronic Engineering, Chongqing University, Chongqing 400044, China. ✉email: qianwang2@pku.edu.cn

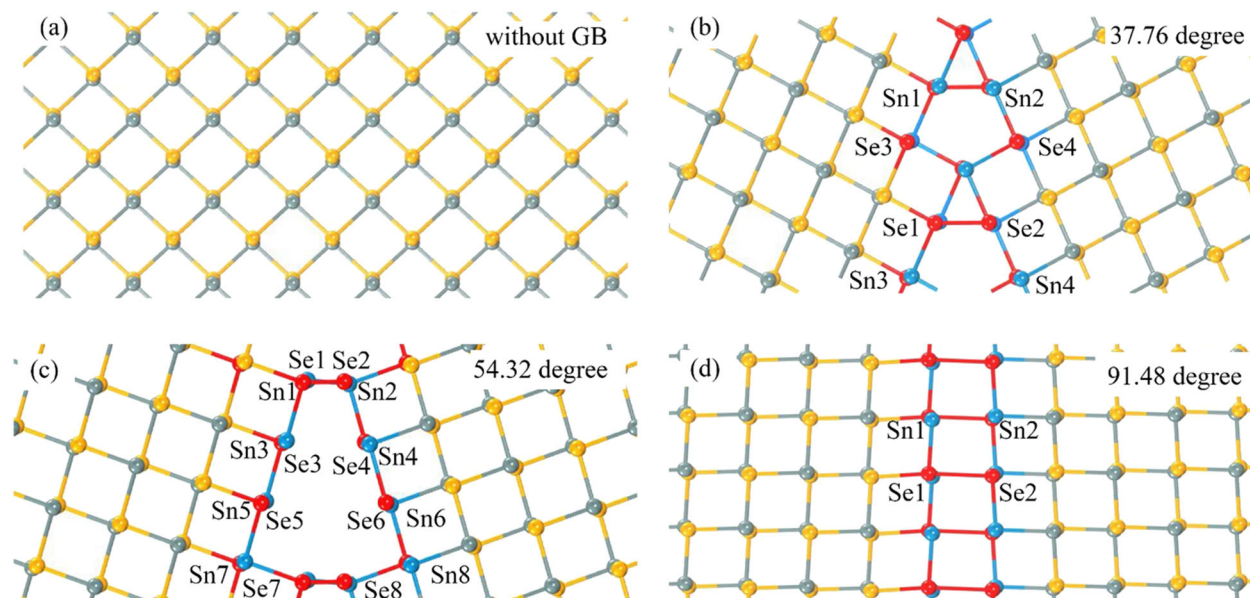


Fig. 1 Geometric structures of 2D SnSe. Top view of the optimized 2D SnSe sheet **a** without GB, with **b** 37.76° GB, **c** 54.32° GB, and **d** 91.48° GB. Red and blue, cyan and yellow spheres represent the Sn and Se atoms in the GBs and grains, respectively.

between two neighboring GBs, we set the distance as 60 Å in calculations. Supplementary Fig. 1b is for the number of atoms versus the distances between two neighboring GBs. Also, to make DFT method handleable for our system, the 2D SnSe with 91.48° GB is chosen for doing the calculations containing 80 Sn and 80 Se atoms with the lattice parameters of $a = 122.78$, $b = 6.14$ Å. The structures with 37.76°/54.32° GB contain 84/62 Sn and 84/62 Se atoms with the lattice parameters of $a = 58.26/62.21$, $b = 13.59/9.63$ Å, respectively. The vacuum space of 18 Å is included along the c directions for these structures. The distances between two neighboring GBs are large enough to avoid their mutual interactions¹⁷. Interestingly, the GB structure with grain orientation angle of 91.48° is similar to the antiphase GB in polycrystalline bulk SnSe discovered by Zhao et al. in the experiment, which is a stable GB type⁴, implying that it is likely to observe such GB type also in 2D SnSe. We calculate the GB energies of the three GB structures using the formula: $E_{GB} = (E_1 - E_0)/2l$, where E_1 and E_0 are the energies of the structures with and without GBs, l is the length of GB. The GB energies of the 2D SnSe with 37.76°, 54.32°, and 91.48° GB are 0.18, 0.34, and 0.21 eV/Å, respectively. Because the structure with 91.48° GB has a similar GB configuration to that of the antiphase GBs in the synthesized polycrystalline SnSe⁴, and the other two GBs are also low in energy, we choose the three configurations for further calculations and discussions.

GBs usually contain some wrong arranged atoms or bonds, as shown in Fig. 1. For the structure with 37.76° GB, the wrong arranged atoms in the GB region are labeled as Sn1–Sn2/Se1–Se2, Sn3–Sn4/Se3–Se4, and for the structure with 54.32° GB, the wrong arranged atoms are labeled as Sn1–Sn2/Se1–Se2, Sn3–Sn4/Se3–Se4, Sn5–Sn6/Se5–Se6, and Sn7–Sn8/Se7–Se8. The situation with wrong arranged atoms in the 91.48° GB is less complicated, shown as Sn1–Sn2 and Se1–Se2.

It was demonstrated that the disordered atoms or some wrong bonds in GBs can result in trapping gap states²³ that are able to trap the carriers and decrease the mobility of free carriers, leading to the reduction of electrical conductivity. For instance, for an n -type semiconductor, these trapping states can be filled by electrons, and when they are accumulated, a negative charge region can be developed in the GB. The adjacent grains of the GB become positively charged and a potential energy barrier is created, thus reducing the mobility of electrons²⁴. While, for those

shallow gap states which are coupled with conducting bands, the potential energy barrier between GB and grain region is low and the detrimental effect can be reduced. To see how GB affects the electronic properties of 2D SnSe, we calculate the band structures of the 2D SnSe with the three GB types, respectively. To avoid the effect caused by the anisotropy of 2D SnSe, the structure without GB for comparison is also tilted by the corresponding degree from the original structure, namely, by 91.48°, as plotted in Supplementary Fig. 2.

Electronic structures

The band structures of the SnSe sheet with and without the 91.48° GB are shown in Fig. 2a, b. To compare the changes of conduction and valence bands, we plot the band structures using band alignment scheme, where the vacuum energy level is set as zero energy. The electrostatic potentials are calculated to be 2.74, 2.73, 2.69, and 2.72 eV for SnSe monolayer without GB, with 91.48° GB, doped with Ge/Si, respectively, as shown in Supplementary Fig. 3. One can see that the GB results in four trapping gap states inside the band gap, which can trap the carriers, leading to the decrease of electrical conductivity. We also calculate the band structures of the 2D SnSe sheets with the 37.76° and 54.32° GB, respectively, as shown in Fig. 3a, d. It is interesting to see the emerging gap states are coupled with the conducting bands for the structure with 54.32° GB. Thus, the carrier mobility is less affected. While, the defect gap states are observed in the structure with the 37.76° GB.

To explore the origins of these gap states, the site-projected DOS of the 2D sheet with 91.48° and 37.76° GB configurations are calculated, respectively. The results are plotted in Supplementary Figs. 4 and 5. For the structure with 91.48° GB, we find four defect gap states arising from the $5p_z$ orbitals of Sn atoms in the GB. Two wrong bonds of Sn–Sn at the middle and another two at the edge are responsible for the four trapping gap states inside the band gap (see Supplementary Fig. 2b). For the structure with 37.76° GB, the defect trapping gap states also originate from the $5p_z$ orbitals of the Sn atoms in the GB. Besides the site-projected DOS, the fat-band analysis is also carried out to study the origins of these emerging gap states inside the band gap. Based on the distance between the GB and Sn, four Sn atoms are chosen for doing the fat-band analysis, as shown in Supplementary Fig. 6. We note when the distance from the GB becomes larger, the contribution

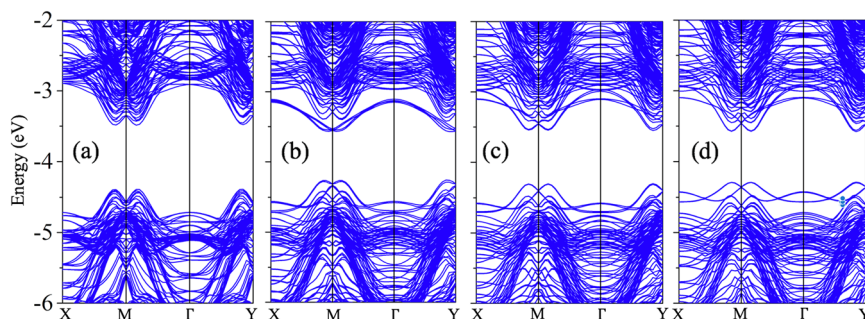


Fig. 2 Band structures of 2D SnSe with 91.48° GB. Band structure of the 2D SnSe sheet **a** without GB and **b** with 91.48° GB, band structure of the **c**, **d** Ge-/Si-doped 2D SnSe sheet with 91.48° GB.

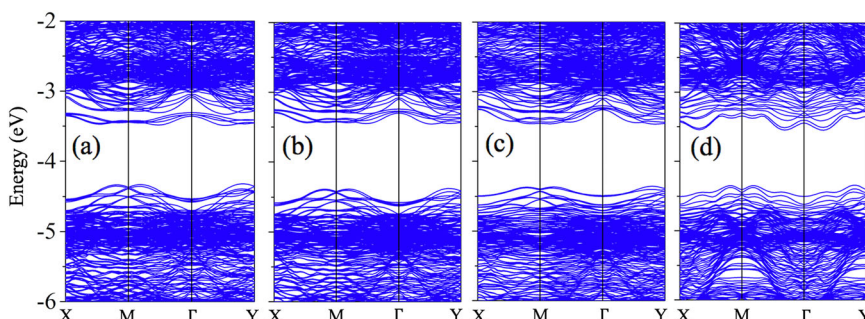


Fig. 3 Band structures of 2D SnSe with 37.76°/54.32° GB. Band structure of **a** the SnSe sheet with 37.76° GB, **b**, **c** the Ge-/Si-doped SnSe sheet with 37.76° GB, and **d** the sheet with 54.32° GB.

to the gap states becomes smaller. Therefore, the emerging gap states are mainly attributed by the Sn atoms around the GB. Supplementary Fig. 7 shows the fat bands when Sn atoms at the GB are replaced by Ge/Si atoms. One can see that the gap states are pushed upwards into the conduction band after doping. Since the trapping gap states are detrimental to electronic transport, a direct strategy to improve electrical conductivity is to eliminate or reduce the trapping gap states. However, less attention was paid on this point in previous studies.

Here, we choose the two GB configurations with 91.48° and 37.76° to study the induced gap states. According to the experiment by Sushmita et al.²⁵, we study the effect of doping Ge in the GB region on the gap states. We first compare the substitution energies of Ge_{Sn} (Ge at Sn site) and Ge_{Se} (Ge at Se site), which are found to -0.32 and $+1.10$ eV, respectively, indicating that Ge prefers to the Sn site. So, the wrong bonds of Sn–Sn become Ge–Ge after the doping. We then examine the Ge segregation energy profile across the GB regions for the two configurations. The results show that the Ge-doping leads to a spontaneous Ge segregation in the GBs, irrespective of the GB types (see Supplementary Fig. 8a). When doped with Ge, the Sn–Sn wrong bonds may become Ge–Ge bonds or Sn–Ge bonds. To find the energetic preference, we calculate their bond energies, which are found to be -0.55 and -0.31 eV for the Ge–Ge and Sn–Ge bonds, respectively, suggesting that forming Ge–Ge bond is energetically more favorable over Sn–Ge bond. The band structure of the Ge-doped sheet with 91.48° GB is plotted in Fig. 2c. One can see that the four trapping gap states are eliminated after the doping. The underlying reason is that the coupling of the $5p_z$ orbitals of Sn in the GB region is changed to the stronger coupling of $4p_z$ orbitals of Ge atoms, which can move the gap states upward to the conduction bands. Thus, the trapping gap states are now eliminated by Ge doping and the potential energy barrier cannot form across the GB. According to the calculated results, the band gap for 91.48° GB with Ge doping is decreased by 0.16 eV, as compared with gap in the pristine situation, due to the

fact that Ge is more electronegative than Sn. We conclude that Ge doping in the GB can eliminate the trapping gap states, resulting in the increased electrical conductivity.

It is natural to consider whether silicon (Si) can also have the similar effect because Si is isoelectronic to Ge and Sn. In addition, Si is much cheaper than Ge. Interestingly, it was found that the power factor and Seebeck coefficient are enhanced when Si is introduced into 3D SnSe¹⁴. Therefore, it is possible to dope SnSe with Si in the experiment. We then dope Si in the 2D SnSe sheet with 91.48° GB. The calculated band structure is plotted in Fig. 2d, which clearly shows that the trapping gap states are eliminated. The corresponding value of band gap reduction is 0.21 eV for the structure with 91.48° GB after Si doping. For the structure with 37.76° GB, we also study the effect of doping on the gap states by replacing Sn with Ge and Si, respectively, in the GB region. The formation energies of Ge and the Si at Sn site are shown in Supplementary Fig. 8b. Again, both Ge and Si are found to have the tendency to occupy the Sn sites in the GB. The band structures are calculated and plotted in Fig. 3b, c, where the trapping gap states turn into shallow gap states coupling with the conducting bands, which are also attributed by the stronger coupling of the $4p_z/3p_z$ orbitals of Ge/Si atoms, as compared with the case of $5p_z$ orbitals of Sn atoms. Therefore, doping Ge/Si in the 2D SnSe with GBs can be a useful strategy to eliminate or reduce the trapping gap states, thus leading to the enhancement of electrical conductivity.

According to the above calculations, one can see that different GB configurations induce the different trapping gap states. From the site-projected DOS of the structures with 37.76° GB and 91.48° GB, we find that the contributions to the total DOS of Sn atoms are related to their distances from the middle of GB. For instance, in Fig. 1b, Sn1–Sn2 contributes more than Sn3–Sn4 to the total DOS. This is understandable because their mutual coupling becomes weaker when the distance between them increases. As shown in Fig. 1b, d, for the structures with 37.76° GB and 91.48° GB, the percentages of wrong arranged atoms with small mutual

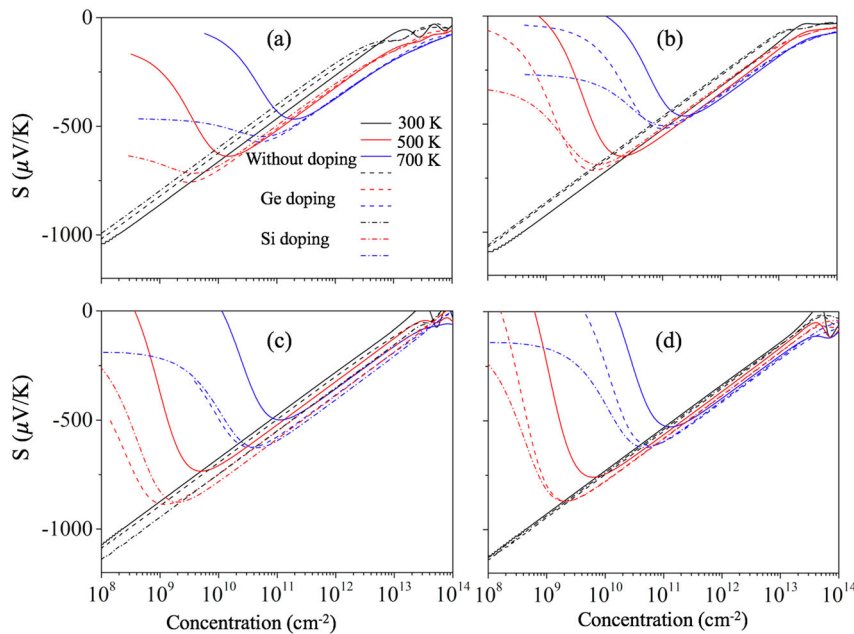


Fig. 4 Seebeck coefficients of n-type 2D SnSe with 91.48° GB. Concentration dependence of the Seebeck coefficients perpendicular **a** and parallel **b** to the GB direction of the n-type 2D SnSe sheet with 91.48° GB. Concentration dependence of the Seebeck coefficients perpendicular **c** and parallel **d** to the GB direction of the n-type 2D SnSe sheet with 37.76° GB, at different temperatures, respectively.

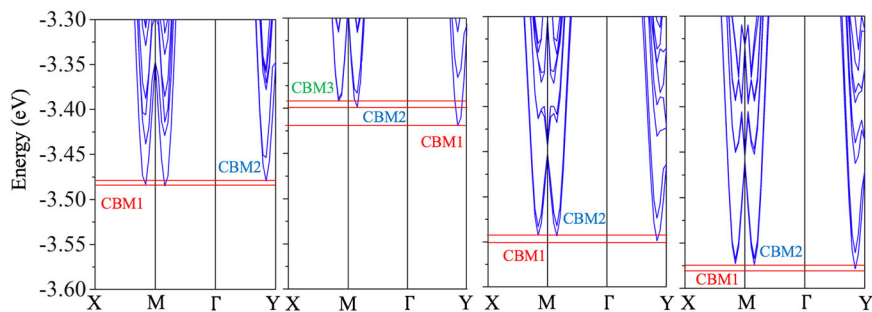


Fig. 5 Band structures of 2D SnSe with 91.48° GB in short energy range. Band structure in a short energy range for the 2D SnSe sheet **a** without GB, **b** with 91.48° GB, and for **c** the Ge-doped and **d** Si-doped SnSe sheet with 91.48° GB.

distances (Sn1–Sn2) are 50% and 100%. While, for the structure with 54.32° GB, the wrong arranged atoms with small distances (Sn1–Sn2 and Sn7–Sn8) occupy 40% of total atoms at GB. The density of wrong bonds with small distances may be not high enough to induce trapping gap states for the structure with 54.32° GB.

Seebeck coefficients

The Seebeck coefficients are then calculated using Boltztrap2 code. Here, we discuss the structures with 37.76° and 91.48° GB, because in both of them trapping gap states are observed. The results for the n-type 2D SnSe are shown in Fig. 4. It is interesting to note that the Seebeck coefficients of the doped sheets increase in both parallel and perpendicular to the GB direction. According to previous studies^{26,27}, we choose the concentration range of 10^8 to 10^{14} cm^{-2} to calculate the Seebeck coefficients. For the structure with 91.48° GB, the Seebeck coefficients at 500/700 K are 641.34/650.25, 470.29/462.65 $\mu\text{V/K}$ in parallel/perpendicular to the GB direction, respectively. When doped with Ge, the corresponding values increase to 759.76/715.62, 574.28/522.92 $\mu\text{V/K}$, as shown in Fig. 4a, b. The calculated results along the x and y directions are close to each other within the numerical error range. It is known that large Seebeck coefficient usually requires

large DOS effective mass (m_d^*), which is related to band effective mass m_b^* and valley degeneracy N_v via $m_d^* = m_b^* N_v^{2/3}$. Therefore, Seebeck coefficient can be tuned by increasing m_b^* or N_v , while they have different effects on carrier mobility μ . The relation between m_b^* and μ is given by $\mu \propto 1/m_b^{*5/2}$, indicating that the increase of m_b^* is detrimental to carrier mobility and the thermoelectric performance. On the other hand, the Seebeck coefficient can be increased by increasing the valley degeneracy, without harming the carrier mobility. The valley degeneracy can be improved by the convergence of many conducting or valance bands, whose energies are close to each other. This strategy has achieved success in improving thermoelectric performance in many materials^{28–33}. To see the conducting bands more clearly, we plot the band structures of 2D SnSe with and without 91.48° GB in small energy ranges, as shown in Fig. 5. From Fig. 5a, for the structure without GB, two degenerate conducting bands can be seen from X to M and M to Γ . The energy difference between CBM1 and CBM2 is only 0.0050 eV. When GB is induced, obvious band divergence can be noted with energy difference between CBM1 and CBM2 becoming 0.0200 eV, as seen in Fig. 5b. Also, the former two degenerate conducting bands from X to M and M to Γ diverge to each other, with energy difference between CBM2 and CBM3 becoming 0.0060 eV. As shown Fig. 5c, d, when the

trapping gap states are eliminated by doping Ge or Si, the conducting bands from X to M and M to Γ converge again and energy differences between CBM1 and CBM2 become 0.0057 and 0.0045 eV, respectively. The vanish of trapping states caused by doping results in the convergence of conducting bands, leading to increase of valley degeneracy. Therefore, the Seebeck coefficients can be enhanced. For the structure with 37.76° GB, those trapping gap states become shallow gap states after doping with Ge, coupling with original conducting bands, as shown in Fig. 3b. The band convergence of these shallow gap states from X to M and M to Γ , compared with the original conducting bands, may account for the increase in the Seebeck coefficients. We then also calculate the Seebeck coefficients of p-type SnSe sheet with and without doping. The results are shown in Supplementary Fig. 9. It is found that Ge doping can also slightly increase the Seebeck coefficients of the structures with 91.48° and 37.76° GB.

Thermal conductivity

Thermal conductivity is another important factor in determining thermoelectric performance of materials. Low thermal conductivity is needed to have a high ZT value. The thermal conductivity of monolayer SnSe was calculated to be 2.5 (2.02) W/mK along the zigzag (armchair) direction in our previous work by solving Boltzmann transport equation combined with DFT calculations¹⁰. In addition, it was experimentally found that the existence of GB and doping atoms can reduce the thermal conductivity of 2D SnSe²⁵ because of the enhanced phonon scattering. So we can expect that the thermal conductivity of 2D SnSe would be reduced by introducing GBs or doping atoms, while its value remains computationally too demanding to be obtained because of the huge supercell. Therefore, the thermoelectric performance of 2D SnSe can be effectively enhanced when GB and doping are incorporated.

Summary

In summary, by studying the effect of GB on the thermoelectric performance of 2D SnSe, we find that different GB configurations can induce different defect trapping gap states inside the band gap, which can form potential energy barrier, thus impeding the mobility of carriers. Such situations can be improved by doping with Ge or Si, which can effectively shift the trapping gap states upper into or close to the conducting bands due to the strong orbital coupling between two Ge or Si atoms, thus enhancing the electrical conductivity. Meanwhile, the band convergence in the conducting bands induced by doping can also increase the Seebeck coefficients of 2D SnSe with GBs. Furthermore, the existence of GB and the Si/Ge dopants can effectively scatter the phonons and decrease the thermal conductivity. These factors together synergistically improve thermoelectric properties of 2D SnSe through GB and doping engineering. These findings can help the design of practical thermoelectric materials that can avoid the problems of single crystal such as the high cost in synthesis and the poor mechanical properties in device processing.

METHODS

Density functional theory calculations

First-principles calculations with the framework of density-functional theory (DFT) are carried out by using the Vienna ab initio simulation package (VASP)^{34,35}, employing the projector augmented wave (PAW) pseudopotentials³⁶. The electron exchange–correlation interaction is treated by using Perdew–Burke–Ernzerhof (PBE) functional³⁷. The energy cutoff is set to 500 eV. The convergence criteria of total energy and final force on each atom during structural optimization are set to be 0.0001 and 0.1 eV/Å. A vacuum space of 18 Å is applied to avoid the interactions between two neighboring layers in the direction perpendicular to the

sheet. The Brillouin zone is sampled with $12 \times 24 \times 1$ Monkhorst–Pack k-point meshes³⁸.

Seebeck coefficients calculations

Electronic transport properties are calculated in the framework of the Boltzmann transport theory within the constant relaxation time approximation. The semiclassical Boltzmann theory as implemented in the Boltztrap2 code³⁹ is used to calculate Seebeck coefficient⁴⁰ defined as

$$S = \frac{e}{\sigma T} \int \tau(\vec{k}) v(\vec{k}) v(\vec{k}) (\epsilon_k - \epsilon_f) \left[-\frac{\partial f^0(\epsilon_k)}{\epsilon_k} \right] d\epsilon \quad (1)$$

where σ represents the electrical conductivity, $\tau(\vec{k})$ is the relaxation time, $v(\vec{k})$ is the group velocity, ϵ_f is the Fermi energy and f^0 is the Fermi-Dirac distribution function. This method has been used successfully to study thermoelectric properties of other 2D materials^{10,26,41}.

DATA AVAILABILITY

The datasets generated and/or analyzed during the current study are available from the corresponding author upon reasonable request.

CODE AVAILABILITY

All code used to calculate the current results is available from the corresponding author upon reasonable request.

Received: 6 January 2020; Accepted: 22 June 2020;

Published online: 15 July 2020

REFERENCES

- Zhao, L.-D. et al. Ultralow thermal conductivity and high thermoelectric figure of merit in SnSe crystals. *Nature* **508**, 373 (2014).
- Chang, C. et al. 3D charge and 2D phonon transports leading to high out-of-plane ZT in n-type SnSe crystals. *Science* **360**, 778–783 (2018).
- Wei, T.-R. et al. Distinct impact of alkali-ion doping on electrical transport properties of thermoelectric p-type polycrystalline SnSe. *J. Am. Chem. Soc.* **138**, 8875–8882 (2016).
- Ge, Z.-H. et al. Boosting the thermoelectric performance of (Na,K)-codoped polycrystalline SnSe by synergistic tailoring of the band structure and atomic-scale defect phonon scattering. *J. Am. Chem. Soc.* **139**, 9714–9720 (2017).
- Chen, Y. X. et al. Understanding of the extremely low thermal conductivity in high-performance polycrystalline SnSe through potassium doping. *Adv. Funct. Mater.* **26**, 6836–6845 (2016).
- Zhang, Q. et al. Studies on thermoelectric properties of n-type polycrystalline SnSe1-xSx by iodine doping. *Adv. Energy Mater.* **5**, 1500360 (2015).
- Chang, C. et al. Raising thermoelectric performance of n-type SnSe via Br doping and Pb alloying. *RSC Adv.* **6**, 98216–98220 (2016).
- Chen, C.-L., Wang, H., Chen, Y.-Y., Day, T. & Snyder, G. J. Thermoelectric properties of p-type polycrystalline SnSe doped with Ag. *J. Mater. Chem. A* **2**, 11171–11176 (2014).
- Luo, Y. et al. High thermoelectric performance in polycrystalline SnSe Via dual-doping with Ag/Na and Nanostructuring With Ag₆SnSe₆. *Adv. Energy Mater.* **9**, 1803072 (2019).
- Wang, F. Q., Zhang, S., Yu, J. & Wang, Q. Thermoelectric properties of single-layered SnSe sheet. *Nanoscale* **7**, 15962–15970 (2015).
- Chen, Y.-X. et al. Understanding of the extremely low thermal conductivity in high-performance polycrystalline SnSe through potassium doping. *Adv. Funct. Mater.* **26**, 6836–6845 (2016).
- Sassi, S. et al. Assessment of the thermoelectric performance of polycrystalline p-type SnSe. *Appl. Phys. Lett.* **104**, 212105 (2014).
- Song, L., Zhang, J. & Iversen, B. B. Enhanced thermoelectric properties of SnSe thin films grown by single-target magnetron sputtering. *J. Mater. Chem. A* **7**, 17981–17986 (2019).
- Ju, H. & Kim, J. Effect of SiC ceramics on thermoelectric properties of SiC/SnSe composites for solid-state thermoelectric applications. *Ceram. Int.* **42**, 9550–9556 (2016).
- Liu, Y. & Yakobson, B. I. Cones, pringles, and grain boundary landscapes in graphene topology. *Nano Lett.* **10**, 2178–2183 (2010).
- Liu, Y., Zou, X. & Yakobson, B. I. Dislocations and grain boundaries in two-dimensional boron nitride. *ACS Nano* **6**, 7053–7058 (2012).

17. Liu, Y., Xu, F., Zhang, Z., Penev, E. S. & Yakobson, B. I. Two-dimensional monoelemental semiconductor with electronically inactive defects: the case of phosphorus. *Nano Lett.* **14**, 6782–6786 (2014).
18. Sangwan, V. K. et al. Gate-tunable memristive phenomena mediated by grain boundaries in single-layer MoS₂. *Nat. Nanotechnol.* **10**, 403 (2015).
19. Ogawa, H. GBstudio: a builder software on periodic models of CSL boundaries for molecular simulation. *Mater. Trans.* **47**, 2706–2710 (2006).
20. Xu, J., Liu, J. B., Liu, B. X., Wang, J. F. & Huang, B. Defect engineering of grain boundaries in lead-free halide double Perovskites for better optoelectronic performance. *Adv. Funct. Mater.* **29**, 11 (2019).
21. Yan, Y. et al. Electrically benign behavior of grain boundaries in polycrystalline CuInSe₂ films. *Phys. Rev. Lett.* **99**, 4 (2007).
22. Yin, W. J. et al. Engineering grain boundaries in Cu₂ZnSnSe₄ for better cell performance: a first-principle study. *Adv. Energy Mater.* **4**, 7 (2014).
23. Seto, J. Y. The electrical properties of polycrystalline silicon films. *J. Appl. Phys.* **46**, 5247–5254 (1975).
24. Bachmann, M., Czerner, M. & Heiliger, C. Ineffectiveness of energy filtering at grain boundaries for thermoelectric materials. *Phys. Rev. B* **86**, 115320 (2012).
25. Chandra, S. & Biswas, K. Realization of high thermoelectric figure of merit in solution synthesized 2D SnSe nanoplates via Ge alloying. *J. Am. Chem. Soc.* **141**, 6141–6145 (2019).
26. Sharma, S., Singh, N. & Schwingenschlogl, U. Two-dimensional tellurene as excellent thermoelectric material. *ACS Appl. Energy Mater.* **1**, 1950–1954 (2018).
27. Li, T. W., Yu, J. B., Nie, G., Zhang, B. P. & Sun, Q. The ultralow thermal conductivity and ultrahigh thermoelectric performance of fluorinated Sn₂Bi sheet in room temperature. *Nano Energy* **67**, 8 (2020).
28. Pei, Y. et al. Convergence of electronic bands for high performance bulk thermoelectrics. *Nature* **473**, 66 (2011).
29. Liu, W. et al. Convergence of conduction bands as a means of enhancing thermoelectric performance of n-type Mg₂Si_{1-x}Snx solid solutions. *Phys. Rev. Lett.* **108**, 166601 (2012).
30. Tan, G. et al. Valence band modification and high thermoelectric performance in SnTe heavily alloyed with MnTe. *J. Am. Chem. Soc.* **137**, 11507–11516 (2015).
31. Tang, Y. et al. Convergence of multi-valley bands as the electronic origin of high thermoelectric performance in CoSb₃ skutterudites. *Nat. Mater.* **14**, 1223 (2015).
32. Tang, J. et al. Maximization of transporting bands for high-performance SnTe alloy thermoelectrics. *Mater. Today Phys.* **9**, 6 (2019).
33. Yao, Z. et al. Solute manipulation enabled band and defect engineering for thermoelectric enhancements of SnTe. *InfoMat* **1**, 571–581 (2019).
34. Kresse, G. & Furthmüller, J. Efficient iterative schemes for ab initio total-energy calculations using a plane-wave basis set. *Phys. Rev. B* **54**, 11169–11186 (1996).
35. Kresse, G. & Furthmüller, J. Efficiency of ab-initio total energy calculations for metals and semiconductors using a plane-wave basis set. *Computational Mater. Sci.* **6**, 15–50 (1996).
36. Blöchl, P. E. Projector augmented-wave method. *Phys. Rev. B* **50**, 17953–17979 (1994).
37. Perdew, J. P., Burke, K. & Ernzerhof, M. Generalized gradient approximation made simple. *Phys. Rev. Lett.* **77**, 3865–3868 (1996).
38. Monkhorst, H. J. & Pack, J. D. Special points for Brillouin-zone integrations. *Phys. Rev. B* **13**, 5188–5192 (1976).
39. Madsen, G. K. H., Carrete, J. & Verstraete, M. J. BoltzTraP2, a program for interpolating band structures and calculating semi-classical transport coefficients. *Comput. Phys. Commun.* **231**, 140–145 (2018).
40. Madsen, G. K. H. & Singh, D. J. BoltzTraP. A code for calculating band-structure dependent quantities. *Comput. Phys. Commun.* **175**, 67–71 (2006).
41. Kim, J. Y. & Grossman, J. C. High-efficiency thermoelectrics with functionalized graphene. *Nano Lett.* **15**, 2830–2835 (2015).

ACKNOWLEDGEMENTS

This work is partially supported by grants from the National Science Foundation China (Grants No. NSFC-21773004 and NSFC-11974028), and the National Key Research and Development Program of the Ministry of Science and Technology of China (Grant No. 2017YFA0205003), and is supported by the High-Performance Computing Platform of Peking University, China. Y.G. acknowledges the Project funded by China Postdoctoral Science Foundation (No. 2019M650289).

AUTHOR CONTRIBUTIONS

Q.W. conceived and designed the project. J.S. performed the calculations of electronic properties. J.S. and J.Y. performed the calculations of Seebeck coefficient. J.S. and Y.G. prepared the structures of SnSe with grain boundaries. All authors contributed to the revisions and discussions of the paper.

COMPETING INTERESTS

The authors declare no competing interests.

ADDITIONAL INFORMATION

Supplementary information is available for this paper at <https://doi.org/10.1038/s41524-020-00368-6>.

Correspondence and requests for materials should be addressed to Q.W.

Reprints and permission information is available at <http://www.nature.com/reprints>

Publisher's note Springer Nature remains neutral with regard to jurisdictional claims in published maps and institutional affiliations.



Open Access This article is licensed under a Creative Commons Attribution 4.0 International License, which permits use, sharing, adaptation, distribution and reproduction in any medium or format, as long as you give appropriate credit to the original author(s) and the source, provide a link to the Creative Commons license, and indicate if changes were made. The images or other third party material in this article are included in the article's Creative Commons license, unless indicated otherwise in a credit line to the material. If material is not included in the article's Creative Commons license and your intended use is not permitted by statutory regulation or exceeds the permitted use, you will need to obtain permission directly from the copyright holder. To view a copy of this license, visit <http://creativecommons.org/licenses/by/4.0/>.

© The Author(s) 2020